Quasi-particle interference probe of the self-energy

2014 New J. Phys. 16 023003

(http://iopscience.iop.org/1367-2630/16/2/023003)

New Journal of Physics
The open access journal at the forefront of physics
Deutsche Physikalische Gesellschaft DPG | IOP Institute of Physics

Quasi-particle interference probe of the self-energy

Thomas Dahm[1] **and D J Scalapino**[2]
[1] Universität Bielefeld, Fakultät für Physik, Postfach 100131, D-33501 Bielefeld, Germany
[2] Physics Department, University of California, Santa Barbara, CA 93106-9530, USA
E-mail: thomas.dahm@uni-bielefeld.de and djs@physics.ucsb.edu

Received 11 October 2013, revised 8 January 2014
Accepted for publication 10 January 2014
Published 4 February 2014
New Journal of Physics **16** (2014) 023003
doi:10.1088/1367-2630/16/2/023003

Abstract
Quasi-particle interference (QPI) measurements have provided a powerful tool for determining the momentum dependence of the gap of unconventional superconductors. Here we examine the possibility of using such measurements to probe the frequency and momentum dependence of the electron self-energy. For illustration, we calculate the QPI response function for a cuprate-like Fermi surface with an electron self-energy from a random phase approximation. Then we try to re-extract the self-energy from the dispersion of the peaks in the QPI response function using different approaches. We show that in principle it is possible to extract the self-energy from the QPI response for certain nested momentum directions. We discuss some of the limitations that one faces.

1. Introduction

Useful information about the interaction of electrons in metals and superconductors is contained in the quasiparticle self-energy $\Sigma(k, \omega)$. When the self-energy and the band structure $E(k)$ of a metal is known, the Green's function $G(k, \omega) = [\omega - E(k) - \Sigma(k, \omega)]^{-1}$ provides complete information on the single particle properties of the system. Experimentally, in isotropic superconducting systems both the normal and anomalous (gap function) self-energies at the Fermi surface can be obtained from tunneling spectroscopy [1]. In anisotropic systems angular resolved photoemission spectroscopy (ARPES) can be used to obtain momentum resolved information on the self-energy [2–7]. In recent years it was shown that the momentum dependence of the gap in unconventional superconductors can be obtained from scanning

tunneling microscopy employing the so-called quasi-particle interference (QPI) [8–16]. In this technique one measures the local tunneling conductance at $\omega = eV$ around an impurity at the surface of a metal over a large grid of points. Its Fourier transform gives a wave vector power spectrum $|\mathrm{Im}\,\Lambda(q,\omega)|^2$. Peaks in $\mathrm{Im}\,\Lambda(q,\omega)$ arise from dynamic nesting processes in which quasi-particles undergo elastic backward scattering from the impurities. From these peaks and their dispersion one can obtain information on nesting properties of the Fermi surface and about the momentum dependence of the superconducting gap [17]. In the present work we want to explore, whether beyond that QPI experiments can be used to also extract information about the momentum and energy dependence of the self-energy, in particular about the effective mass and the lifetime of the quasiparticles. The main idea here is to closely investigate the dispersion and the width of the peaks in $\mathrm{Im}\,\Lambda(q,\omega)$ as a function of energy ω and try to extract the self-energy from it. We will demonstrate that in principle this is possible and we will discuss some of the limitations that one faces.

In a metal, the dispersion and damping of quasi-particles with energy ω is described by a complex frequency dependent wave vector $k(\omega) = k_1(\omega) + \mathrm{i}k_2(\omega)$, where $k_1(\omega)$ determines the renormalized dispersion and $k_2(\omega)$ the lifetime of a quasiparticle state. The band structure $E(k)$ and the self-energy $\Sigma(k,\omega)$ determine $k(\omega)$ and conversely, given $E(k)$, the structure of the self-energy is reflected in $k_1(\omega)$ and $k_2(\omega)$. The tunneling conductance at a particular point depends upon $k(\omega)$ and the surrounding impurity configuration. Here we will discuss how one can extract $k(\omega)$ from the structure in $\mathrm{Im}\,\Lambda(q,\omega)$ and use it to study the real and imaginary parts of the self-energy.

2. Peaks in the quasi-particle interference (QPI) response

For weak charge impurity scattering, the wave-vector power spectrum of the local tunneling density of states depends upon the product of a static impurity structure factor and the QPI response function. Neglecting vertex corrections, the response function can be written as [17]

$$\Lambda(q,\omega) = \int \mathrm{d}^2x\, \mathrm{e}^{\mathrm{i}\mathbf{q}\cdot\mathbf{x}} G(x,\omega)G(-x,\omega) \tag{1}$$

with $\omega = eV$. An expression for $\Lambda(q,\omega)$ including vertex corrections is given in [18]. Here we consider the QPI response for a given value of ω plotted as a function of wave-vector q along certain lines in the Brillouin zone called q-cuts [11]. Examples of such q-cuts are illustrated in figure 1 for a two-dimensional (2D) free electron system and in figure 2(a) for a cuprate-like band structure. Along a q-cut, the QPI response function $\mathrm{Im}\,\Lambda(q,\omega)$ peaks near wave-vectors $q_{\mathrm{peak}}(\omega)$ which connect equi-energy quasi-particle surfaces which have oppositely directed quasi-particle velocities. As noted, these peaks reflect a dynamic nesting which depends on the band structure $E(k)$ as well as the quasi-particle self-energy. For the 2D free electron case the radial q-cuts all give the same information, while for the cuprate-like bandstructure the horizontal q-cut (c) shown in figure 2(a) probes the antinodal region of the Fermi surface while the diagonal q-cuts probe both the nodal (a) as well as intermediate regions (b), which depend on ω, as shown in figures 2(b) and (c).

As we will discuss, by fitting the ω dependence of the peak structure in the QPI, one can extract information on the ω dependence of the real and imaginary parts of the self-energy. Both normal and Umklapp peaks associated with a given q-cut provide similar information and in principle the Umklapp peaks can be used to estimate the q dependent fall-off of the impurity scattering structure factor.

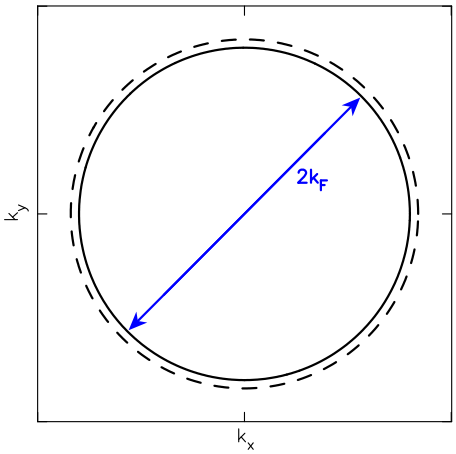

Figure 1. A q-cut passing through the Fermi surface of a 2D free electron system. For $\omega = 0$, $q = 2k_F$ leads to nesting, while for $\omega = 0.1\mu$ (dashed circle) nesting occurs for $q = 2k(\omega) = 2k_F\sqrt{1.1}$.

To begin, we consider the 2D free electron system of figure 1. In this case

$$G(x, \omega) \simeq -i\pi N(0) H_0^{(1)}(k(\omega)r) \tag{2}$$

with $H_0^{(1)}$ the zeroth order Hankel function of the first kind [17], $N(0)$ the single particle density of states, and $k(\omega)$ is determined from the dispersion relation

$$\omega = \frac{k^2(\omega)}{2m} - \mu. \tag{3}$$

Here $\mu = k_F^2/2m$. Carrying out the spatial integration in equation (1), the QPI response function

$$-\frac{1}{\pi}\mathrm{Im}\,\Lambda(q, \omega) = \frac{8\pi N^2(0)}{q}\mathrm{Re}\,\frac{1}{\sqrt{q^2 - (2k(\omega))^2}} \tag{4}$$

is found to have a square-root singularity for

$$q = 2k(\omega) = 2\frac{k}{F}\sqrt{1 + \frac{\omega}{\mu}} \simeq 2\left(k_F + \frac{\omega}{v_F}\right). \tag{5}$$

This wave-vector connects nested equi-energy contours at $k(\omega)$ and $-k(\omega)$ along the q-cut. When impurity scattering is taken into account

$$k(\omega) \simeq k_F + \frac{\omega}{v_F} + \frac{i}{2\ell} \tag{6}$$

with ℓ the mean free path. In this case the wave vector $k(\omega) = k_1(\omega) + ik_2(\omega)$ contains information on both the real and imaginary parts of the single particle propagation.

3. Random phase approximation self-energy

For an interacting system, again neglecting vertex corrections

$$\Lambda(q, \omega) = \int \frac{d^2k}{(2\pi)^2} G(k, \omega) G(k + q, \omega) \tag{7}$$

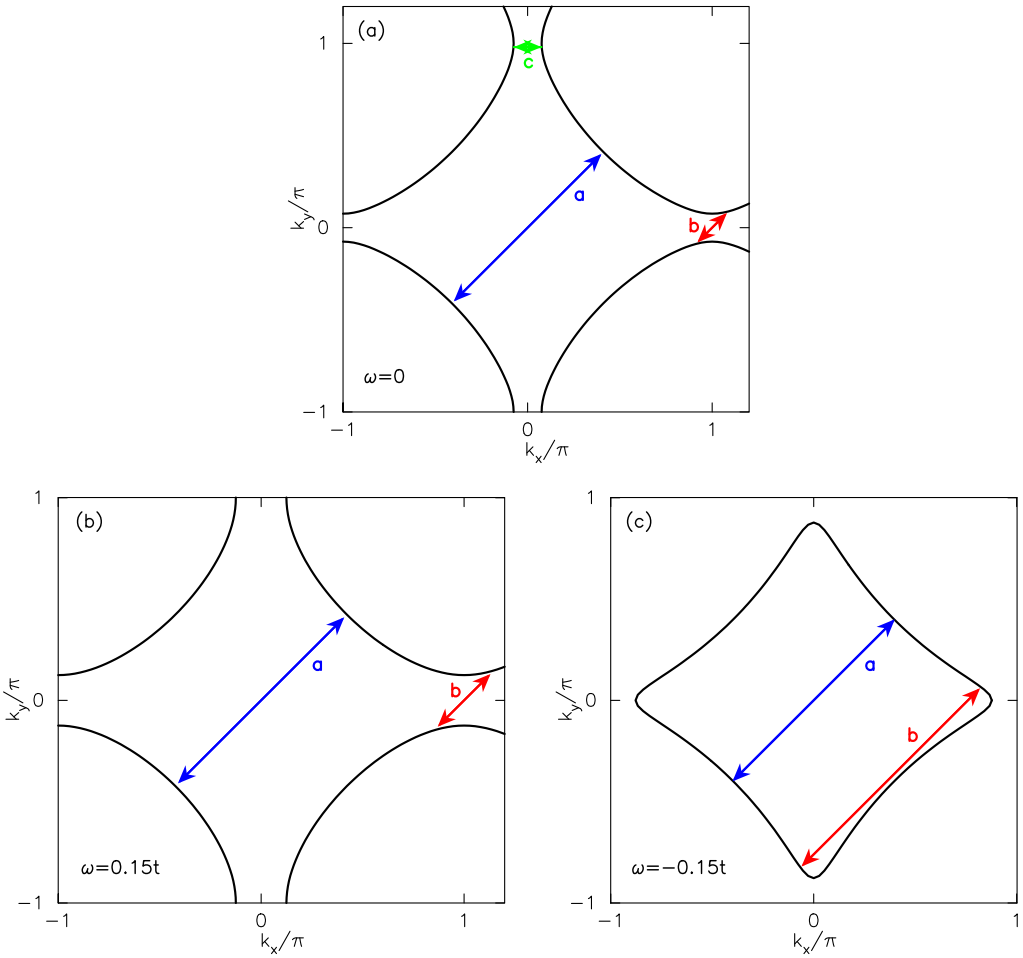

Figure 2. (a) Diagonal and horizontal q-cuts for a cuprate-like Fermi surface. In diagonal direction nesting occurs for q_a and q_b, while in horizontal direction nesting occurs for q_c. (b) The $k(\omega)$ surface for $\omega = 0.15t$ with diagonal q-cuts which nest for q_a and q_b. (c) Similar to (b) for $\omega = -0.15t$. Here, the nesting vector q_b has changed due to the change of topology of the $k(\omega)$ surface.

with

$$G(k,\omega) = [\omega Z(k,\omega) - E(k)]^{-1}. \tag{8}$$

We have set $\Sigma(k,\omega) = (1 - Z(k,\omega))\omega$ and $E(k)$ is the bandstructure energy minus the chemical potential μ. For illustration, we will calculate $Z(k,\omega) = Z_1(k,\omega) + iZ_2(k,\omega)$ for a Hubbard model using a random phase approximation (RPA) for the spin-fluctuation interaction [19]

$$(1 - Z(k,\omega))\,\omega = -\int \frac{d\omega}{\pi} \int \frac{d^2q}{(2\pi)^2} G_0(k+q, \omega+\Omega) \frac{3}{2} \frac{\bar{U}^2 \chi_0(q,\Omega)}{1 - U\chi_0(q,\Omega)}, \tag{9}$$

$$\chi_0(q,\Omega) = \int \frac{d\omega}{2\pi} \int \frac{d^2k}{(2\pi)^2} G_0(k+q, \omega+\Omega) G_0(k,\omega). \tag{10}$$

Here, $G_0(k,\omega) = [\omega - E(k) + \delta\,\mathrm{sgn}(\omega)]^{-1}$ with a tight-binding bandstructure

$$E(k) = -2t(\cos k_x + \cos k_y) - 4t' \cos k_x \cos k_y - 2t'' \cos 2k_x \cos 2k_y - \mu \tag{11}$$

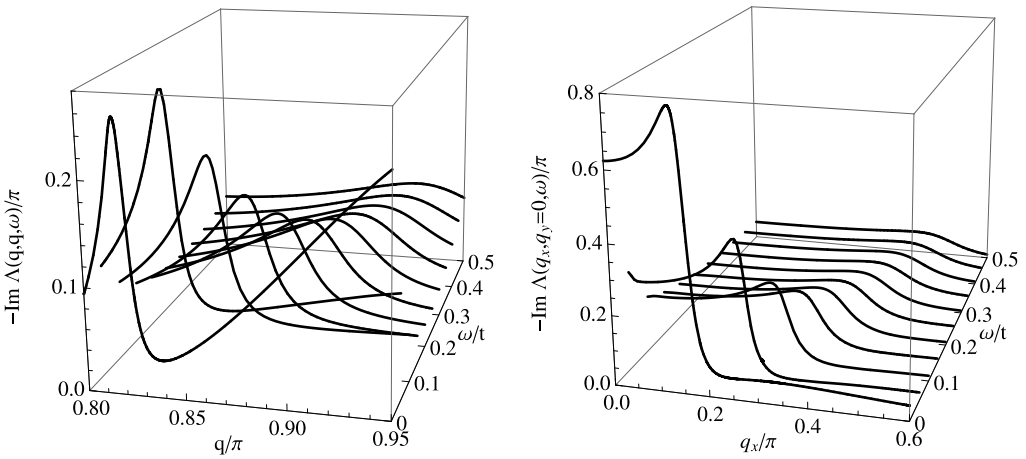

Figure 3. Plots of $-\frac{1}{\pi}\mathrm{Im}\,\Lambda(q,\omega)$ versus q for ω/t values separated by 0.05 for the diagonal (a) and horizontal (b) q-cuts of figure 2(a). As ω/t increases the QPI peak disperses and broadens.

and $t'/t = -0.15$, $t''/t = 0.075$, $\mu/t = -0.81$. The parameters of the bandstructure were taken from tight-binding fits to ARPES data appropriate for the $La_{2-x}Sr_xCuO_4$ cuprate near optimum doping $x = 0.15$ [20]. The coupling constants $\bar{U}/t = 3$ and $U/t = 1.5$ have been chosen such that a mass renormalization of $Z_1(\omega = 0) \approx 2$ is obtained at the nodal direction and $Z_1(\omega = 0) \approx 3$ at the antinodal direction. For the numerical calculations a finite broadening of $\delta = 0.005t$ has been used.

Calculating the RPA self-energy $Z(k,\omega)$ for these parameters and using it in equation (7), we find the QPI response shown in figure 3. In the following we will consider $-\frac{1}{\pi}\mathrm{Im}\,\Lambda(q,\omega)$ as our 'experimental' QPI response and explore how one can extract information about $Z(k,\omega)$ from it.

4. Estimation of the self-energy from the peak position

From figure 3, one sees that the response is characterized by a peak which disperses and broadens as ω/t increases. The peak in figure 3(a) corresponds to the nesting vector 'a' in figure 2(a), while the peak in figure 3(b) corresponds to the nesting vector 'c' in figure 2(a). There exists another peak along the diagonal q-cut at smaller values of q, which corresponds to the nesting vector 'b' in figure 2(a), but is not shown here. We do not consider the nesting vector 'b' any further, as in the case discussed here it gives similar information about the self-energy for antinodal momenta as vector 'c'.

Within a quasi-particle approximation, one finds that the peaks have similar structure to equation (4)

$$-\frac{1}{\pi}\mathrm{Im}\,\Lambda(q,\omega) \sim \mathrm{Re}\,\frac{1}{\sqrt{2k(\omega)-q}} \tag{12}$$

with $k(\omega) = k_1(\omega) + \mathrm{i}k_2(\omega)$ determined by

$$Z_1\left(k_1(\omega),\omega\right) = \frac{E\left(k_1(\omega)\right)}{\omega} \tag{13}$$

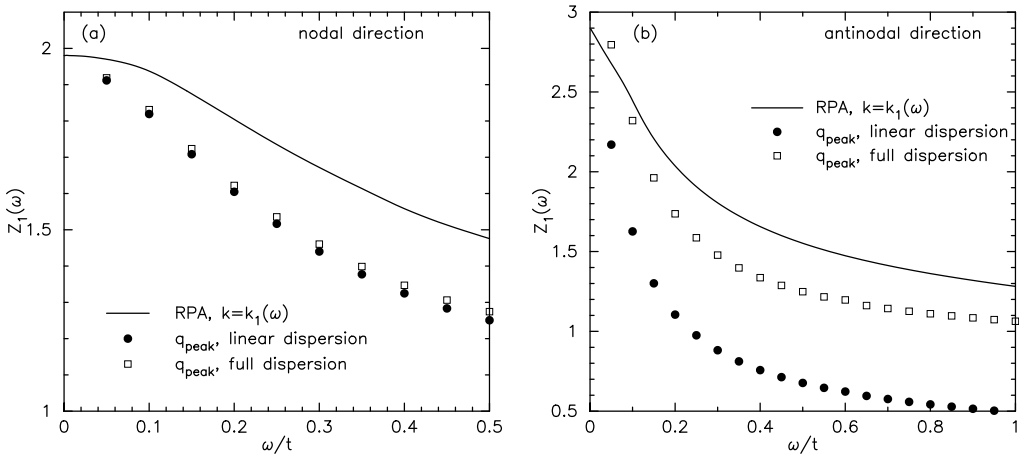

Figure 4. Comparison of $E(q_{\rm peak}(\omega)/2)/\omega$ (open squares) and its linear form $v_{\rm F}(q_{\rm peak}(\omega)/2 - k_{\rm F})/\omega$ (solid circles) with $Z_1(k_1(\omega), \omega)$ (solid curve) for (a) nodal and (b) antinodal q-cuts.

and

$$\omega Z_2\left(k_1(\omega), \omega\right) = v_{\rm F}\left(k_1(\omega)\right) k_2(\omega). \tag{14}$$

Here, $v_{\rm F}(k_1(\omega)) = \frac{\partial E}{\partial k_\perp}(k_1(\omega))$ is the band velocity with the derivative taken perpendicular to the surface where the q-cut crosses the $\omega = E(k_1(\omega))$ surface. The change in sign of the wave vectors in the square-root of equation (12) relative to equation (4) arises from the change in sign of the Fermi surface curvature.

If one takes the peak value $q_{\rm peak}(\omega)$ as an estimate of $2k_1(\omega)$, neglects the imaginary part and uses a linearized dispersion $E(k_1(\omega)) \approx v_{\rm F}(k_1(\omega) - k_{\rm F})$ one finds approximately

$$Z_1(k_{\rm F}, \omega) \simeq \frac{v_{\rm F}}{\omega}\left(\frac{q_{\rm peak}(\omega)}{2} - k_{\rm F}\right). \tag{15}$$

If $q_{\rm peak}(\omega)$ exceeds the region over which a linear approximation of the dispersion is appropriate, then one needs to use the full dispersion and

$$Z_1(k_{\rm F}, \omega) \simeq \frac{E\left(q_{\rm peak}(\omega)/2\right)}{\omega}. \tag{16}$$

In figure 4 the results for $Z_1(\omega)$ obtained using $q_{\rm peak}(\omega)/2$ as an estimate of $k_1(\omega)$ for both the diagonal and horizontal q-cuts are compared with $Z_1(k_1(\omega), \omega)$ (solid curves) obtained from equation (9). For the nodal direction, $E(k)$ is well approximated by its linearized $v_{\rm F}(k - k_{\rm F})$ form while for the antinodal direction a linear approximation fails due to the closeness of the Fermi level to the saddle point of the band at $(0, \pi)$. In this case it is necessary to use the full band dispersion $E(k)$. In both cases, using $q_{\rm peak}(\omega)$ underestimates $2k_1(\omega)$ and the resulting $Z_1(\omega)$ falls below the self-energy used in the calculation of $\Lambda(q, \omega)$.

5. Fitting of the QPI peaks

The problem with using the peak of the QPI q-cut to estimate $Z_1(\omega)$ is that $k(\omega)$ in equation (12) has both real and imaginary parts. Thus a better alternative is to fit the QPI peak to the

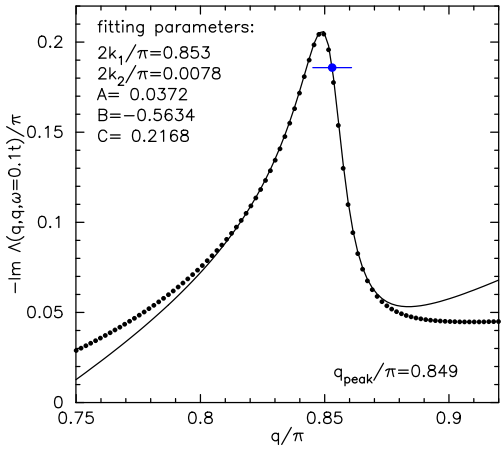

Figure 5. Fitting $-\frac{1}{\pi}\mathrm{Im}\,\Lambda(q,\omega=0.1t)$ along a diagonal q-cut using equation (17) to obtain $k_1(\omega)$ and $k_2(\omega)$.

square-root form of equation (12) and extract a $k_1(\omega)$ and $k_2(\omega)$ for each ω q-cut. Figure 5 shows the results of a fit to a form

$$-\frac{1}{\pi}\mathrm{Im}\,\Lambda(q,\omega)=\mathrm{Re}\,\frac{A}{\sqrt{2k_1(\omega)+\mathrm{i}2k_2(\omega)-q}}+B+Cq. \tag{17}$$

Here, $\omega=0.1t$ along a diagonal q-cut is shown. A finite q range of $[0.825, 0.875]\,\pi$ has been used for the fitting. As can be seen in figure 3 the peaks for a cuprate-like bandstructure appear to have a linear 'background' behind the smeared square-root singularity. For that reason we found it necessary to include a linear background $B+Cq$ in the fitting formula equation (17), which improves the determination of k_1 and k_2. The blue dot in figure 5 denotes the position of the extracted $2k_1$ and the blue bar the width $\pm 2k_2$ for this particular energy ω. As this plot shows, the actual position of $2k_1$ is slightly off from the peak position q_{peak} to the right. The reason for this is the asymmetric line shape of the square-root singular QPI response function equation (12). As seen below, the fitted values of k_1 and k_2 allow a much more precise extraction of Z_1 and Z_2 than the peak position $q_{\mathrm{peak}}/2$.

To get precise values of k_1 and k_2 from the fit we found it necessary to restrict the fitting to a finite q range around the peak position to avoid the fit being spoiled by values away from the peak, where the fitting formula equation (17) is not valid anymore. To get a good coverage of the peak we have chosen the following q ranges: $[q_{\mathrm{peak}}-0.02\pi(1+|\omega|/t), q_{\mathrm{peak}}+0.02\pi(1+2|\omega|/t)]$ in the nodal direction and $[q_{\mathrm{peak}}-0.02\pi(1+4|\omega|/t),\ q_{\mathrm{peak}}+0.02\pi(1+8|\omega|/t)]$ in the antinodal direction. These q ranges account for a minimum range of $\Delta q=0.04\pi$, they increase with increasing $|\omega|$ to account for the fact that the peaks are getting broader at higher frequencies, and the larger range in the antinodal direction accounts for the smaller Fermi velocity in this direction which leads to larger peak widths. Also note that we have chosen the q range asymmetrically around the peak position, as $2k_1$ is always larger than q_{peak}.

After $k_1(\omega)$ and $k_2(\omega)$ have been extracted from these fits, for the linear dispersion approximation we will compare

$$v_{\mathrm{F}}(k_1(\omega)-k_{\mathrm{F}})/\omega \tag{18}$$

and

$$v_{\mathrm{F}}k_2(\omega) \tag{19}$$

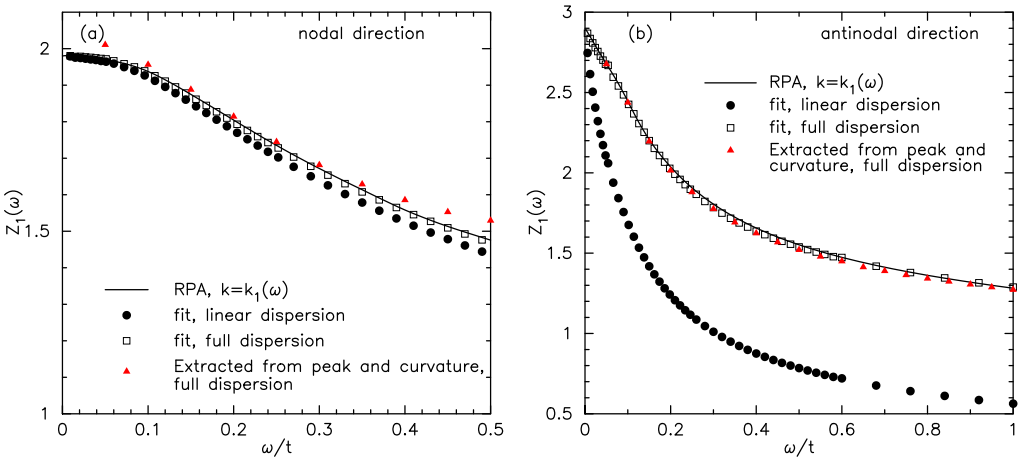

Figure 6. Comparisons of $E(k_1(\omega))/\omega$ (open squares) and its linearized form $v_F(k_1(\omega) - k_F)/\omega$ (solid circles) with $Z_1(k_1(\omega), \omega)$ (solid curve) for (a) nodal and (b) antinodal q-cuts. Here $k_1(\omega)$ used in $E(k_1(\omega))$ and $v_F(k_1(\omega) - k_F)$ is obtained from fitting equation (17). The (red) triangles are obtained when $k_1(\omega)$ is extracted using the peak and normalized curvature, equations (22) and (23).

with $Z_1(k_1(\omega), \omega)$ and $\omega Z_2(k_1(\omega), \omega)$, respectively. In the following all of our estimates will be compared with $Z(k_1(\omega), \omega)$ since the self-energy does have a weak k dependence. If the dynamic range is such that the nonlinearity of the dispersion is important, then the comparison will be with

$$Z_1(k_1(\omega), \omega) = E(k_1(\omega))/\omega \tag{20}$$

and

$$\omega Z_2(k_1(\omega), \omega) = \left(\frac{\partial E}{\partial k_\perp}(k_1(\omega))\right) k_2(\omega). \tag{21}$$

In the following plots, the solid curves are the RPA self-energy evaluated at $k = k_1(\omega)$ with $k_1(\omega)$ in this case obtained from the self-energy calculation equation (9). Our goal is to see how well one can extract the solid curves from the QPI response $-\frac{1}{\pi}\mathrm{Im}\,\Lambda(q, \omega)$.

As shown in figures 6(a) and 7(a) for the nodal case, useful estimates of $Z_1(k_1(\omega), \omega)$ and $Z_2(k_1(\omega), \omega)$ can be obtained using $(k_1(\omega), k_2(\omega))$ and a linear approximation of the dispersion. Similarly in figures 6(b) and 7(b) one sees that if $(k_1(\omega), k_2(\omega))$ can be extracted by fitting $\mathrm{Im}\,\Lambda(q, \omega)$ for the antinodal case one can again obtain useful estimates of the self-energy. However, in the antinodal case it is important to use the full bandstructure $E(k)$.

6. Extraction using peak position and normalized curvature

While fitting $\mathrm{Im}\,\Lambda(q, \omega)$ with equation (17) provides a way of extracting $k_1(\omega)$ and $k_2(\omega)$, as well as supports the validity of the approximation equation (12) near the peak position, one would like to have a more direct procedure, which avoids choosing a finite q range for the fit. From equation (12) one finds that the peak occurs for

$$q_{\mathrm{peak}} = 2k_1(\omega) + 2k_2(\omega)/\sqrt{3} \tag{22}$$

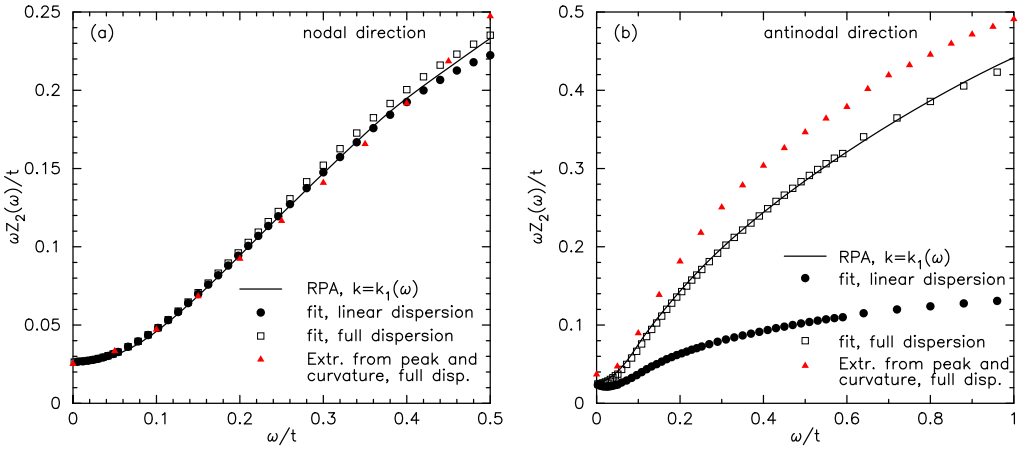

Figure 7. Comparisons of $\frac{\partial E}{\partial k_\perp}(k_1(\omega))k_2(\omega)$ (open squares) and its linearized form $v_F k_2(\omega)$ (solid circles) with $\omega Z_2(k_1(\omega), \omega)$ (solid curve) for (a) nodal and (b) antinodal q-cuts. Here $k_1(\omega)$ and $k_2(\omega)$ were obtained by fitting equation (17). The (red) triangles were again obtained using $k_1(\omega)$ and $k_2(\omega)$ extracted using the peak and normalized curvature.

and at the peak, the normalized curvature

$$\frac{\frac{d^2 \mathrm{Im}\,\Lambda(q,\omega)}{dq^2}|_{q_{\mathrm{peak}}}}{\mathrm{Im}\,\Lambda(q_{\mathrm{peak}},\omega)} = -\frac{9}{16}\frac{1}{(2k_2)^2}. \tag{23}$$

Results obtained for Z_1 and Z_2 using equations (22) and (23) are shown as the red triangles in figures 6 and 7. While this way of extracting $k_1(\omega)$ and $k_2(\omega)$ from the QPI response is less accurate than fitting equation (17), it can provide reasonable results. The $B + Cq$ background must be removed from $\mathrm{Im}\,\Lambda(q,\omega)$ in estimating the normalized curvature, equation (23).

7. Conclusions

While we have been able to extract from $\mathrm{Im}\,\Lambda(q,\omega)$ the self-energy that went into the Green's functions used to calculate it, these results illustrate some of the challenges and limitations one faces. Extracting $k_1(\omega)$ and $k_2(\omega)$ will clearly become more difficult as ω increases and the peak broadens and decreases in amplitude[3]. As seen for the diagonal $k_x = k_y$ cut in figure 2, there can also be multiple peaks associated with a given q-cut. For $\omega > 0$, these peaks are well separated in q. However, as seen in figure 2(c), for this Fermi surface there are problems for $\omega < 0$, where the q_a and q_b peaks approach each other for $\omega < 0$. In addition to $k_1(\omega)$ and $k_2(\omega)$ we used information on the bare bandstructure $E(k)$ which is not a measured quantity. For the diagonal q-cut it appears that the band Fermi velocity v_F would be sufficient, and in principle one might hope that at large values of ω one could estimate the bare v_F. However, by these energies one is typically out of the linear region of dispersion. Thus one needs to make a reasonable estimate for $E(k)$ based on band theory.

[3] By going into the superconducting state one can obtain a sharper response. In this case one will need to take into account the superconducting gap. However at energies large compared with $|\Delta(k)|$ the corrections to Z will be of order $|\Delta/\omega|^2$.

Finally, there is the q-dependence of the impurity scattering form factor and the effect of vertex corrections [18]. The scattering form factor will reduce the amplitude of the QPI response as q increases but should not lead to significant shifts of the $k_1(\omega)$ and $k_2(\omega)$ values provided its characteristic momentum is large compared with $k_2(\omega)$. While the vertex $\Gamma(k, q)$ can introduce additional structure, the continuity of the peak associated with the interference between the two propagators as ω increases along with the short range nature of the vertex corrections should generally limit its effect on $k_1(\omega)$ and $k_2(\omega)$.

Acknowledgments

DJS acknowledges the support of the Center for Nanophase Materials Science at ORNL, which is sponsored by the Division of Scientific User Facilities, US DOE. TD acknowledges support for the Article Processing Charge by the Deutsche Forschungsgemeinschaft and the Open Access Publication Funds of Bielefeld University Library.

References

[1] McMillan W L and Rowell J M 1969 in *Superconductivity* vol 1 ed R D Parks (New York: Dekker) chapter 11 pp 561–613
[2] Valla T, Fedorov A V, Johnson P D, Wells B O, Hulbert S L, Li Q, Gu G D and Koshizuka N 1999 *Science* **285** 2110
[3] Bogdanov P V *et al* 2000 *Phys. Rev. Lett.* **85** 2581
[4] Kaminski A, Randeria M, Campuzano J C, Norman M R, Fretwell H, Mesot J, Sato T, Takahashi T and Kadowaki K 2001 *Phys. Rev. Lett.* **86** 1070
[5] Kaminski A and Fretwell H M 2005 *New J. Phys.* **7** 98
[6] Yun J H, Bok J M, Choi H Y, Zhang W, Zhou X J and Varma C M 2011 *Phys. Rev.* B **84** 104521
[7] Zhang W *et al* 2012 *Phys. Rev.* B **85** 064514
[8] Byers J M, Flatté M E and Scalapino D J 1993 *Phys. Rev. Lett.* **71** 3363
[9] Petersen L, Sprunger P T, Hofmann P, Lægsgaard E, Briner B G, Doering M, Rust H-P, Bradshaw A M, Besenbacher R and Plummer E W 1998 *Phys. Rev.* B **57** R6858
[10] Hoffman J E, McElroy K, Lee D-H, Lang K M, Eisaki H, Uchida S and Davis J C 2002 *Science* **297** 1148
[11] Hanaguri T, Kohsaka Y, Davis J C, Lupien C, Yamada I, Azuma M, Takano M, Ohishi K, Ono M and Takagi H 2007 *Nature Phys.* **3** 865
[12] Hanaguri T, Kohsaka Y, Ono M, Maltseva M, Coleman P, Yamada I, Azuma M, Takano M, Ohishi K and Takagi H 2009 *Science* **323** 923
[13] Hänke T *et al* 2012 *Phys. Rev. Lett.* **108** 127001
[14] Allan M P, Rost A W, Mackenzie A P, Xie Y, Davis J C, Kihou K, Lee C H, Iyo A, Eisaki H and Chuang T-M 2012 *Science* **336** 563
[15] Fujita K, Schmidt A R, Kim E-A, Lawler M J, Lee D H, Davis J C, Eisaki H and Uchida S 2012 *J. Phys. Soc. Japan* **81** 011005
[16] Allan M P, Massee F, Morr D K, Van Dyke J, Rost A W, Mackenzie A P, Petrovic C and Davis J C 2013 *Nature Phys.* **9** 468
[17] Wang Q H and Lee D H 2003 *Phys. Rev.* B **67** 020511
Capriotti L, Scalapino D J and Sedgewick R D 2003 *Phys. Rev.* B **68** 014508
[18] Kivelson S A, Bindloss I P, Fradkin E, Oganesyan V, Tranquada J M, Kapitulnik A and Howald C 2003 *Rev. Mod. Phys.* **75** 1201
[19] Dahm T, Hirschfeld P J, Scalapino D J and Zhu L 2005 *Phys. Rev.* B **72** 214512
[20] Yoshida T *et al* 2007 *J. Phys.: Condens. Matter* **19** 125209